Influence of Ru Doping on the Structure, Defect Chemistry, Magnetic Interaction, and Carrier Motion of the $La_{1-x}Na_xMnO_{3+\delta}$ Manganite

Lorenzo Malavasi,*,† Maria Cristina Mozzati,‡ Cristina Tealdi,† Carlo Bruno Azzoni,‡ and Giorgio Flor†

Dipartimento di Chimica Fisica "M. Rolla", INSTM, IENI/CNR Unità di Pavia of Università di Pavia, V.le Taramelli 16, I-27100 Pavia, Italy, and CNISM and Dipartimento di Fisica "A. Volta", Università di Pavia, Via Bassi 6, I-27100 Pavia, Italy

Received: May 10, 2005; In Final Form: September 9, 2005

In this work, we report a structural, electrical, and magnetic characterization of the $La_{1-x}Na_xMn_{1-y}Ru_yO_{3+\delta}$ (LNMRO) system with $x = 0.05$ and 0.15 and $y = 0$, 0.05, and 0.15, also comprising an investigation of the role of the oxygen content on the related redox properties. The experimental investigation has been realized with the aid of X-ray powder diffraction, electron microprobe analysis, thermogravimetry, electrical resistivity and magnetization measurements, and electron paramagnetic resonance. We demonstrate that the effect of ruthenium doping on the studied LNMRO compounds is not only directly related to the Ru/Mn substitution and to the Ru oxidation state but also indirectly connected to the oxygen content in the sample. Our data show that ruthenium addition can "improve" electrical and magnetic properties of nonoptimally (low) cation-doped manganites, causing an increase of the T_C value and the insurgence of magnetoresistance effect, as observed for the $x = 0.05$ and $y = 0.05$ sample (MR ≅ 60% at 7 T and at ∼260 K).

1. Introduction

Strong interest has been triggered, in recent years, by the possibility of tuning the structural, magnetic, and electrical properties of mixed-valent manganite perovskites by cation doping on the Mn site so that new peculiar features were discovered as the appearance of a metallic-like state and of ferromagnetism in insulating and antiferromagnetic manganites when doped with chromium,[1,2] cobalt,[3] nickel,[3] or ruthenium.[4−8] This effect was connected to the "collapse" of the charge and orbital ordering of Mn^{3+} and Mn^{4+} ions.

It was shown by Vertuyen et al.[8] that Ni^{2+} substitution in $LaMnO_3$ induces double exchange Mn^{3+}/Mn^{4+} ferromagnetic (FM) interactions competing with the Mn^{3+}/Mn^{3+} antiferromagnetic (AF) superexchange interactions: Ni^{2+} substitution takes place directly in the exchange interactions, leading to a stabilization of the FM ground state. Other "new" phenomena have been found in Cr-doped manganites. For the $Pr_{0.5}Ca_{0.5}Mn_{0.99}Cr_{0.01}O_3$ compound, Raveau et al.[2] reported about a "spectacular" resistivity increase in a 4 T magnetic field; also in this case, the main reasons were the partial destruction of the charge ordering and phase separation.

Among the several possible dopants, one of the most studied is ruthenium. The main reasons for this can be summarized as follows: (i) a large amount of Ru can be introduced within the perovskite network keeping it single-phase; (ii) Ru can exhibit different oxidation states (Ru^{3+}, Ru^{4+}, and Ru^{5+}); (iii) the Ru^{3+} and Ru^{4+} low-spin configurations make this dopant suitable for FM coupling with the Mn ions, thus preserving and participating in the double-exchange mechanism.

Ru substitution can induce, over a very large composition range,[4] metallic behavior and FM in AF materials irrespective to the exact nature of the AF order. However, until now, several "anomalies" in the metallic (M) and FM state of Ru-doped manganites are far from being understood; among them, we can cite the small values of the experimental magnetic moment (even in high magnetic fields) with respect to the calculated ones and the "double bump" in the resistivity curves $\rho(T)$. Some argumentation is given in the current literature to explain all, or at least some, of the features cited above. Raveau et al.[4] argue that Ru substituted for Mn is in the +5 valence state, in agreement with other experimental results,[9] and consequently the doping will increase the Mn^{3+} content according to

$$2Mn^{4+} \rightarrow Ru^{5+} + Mn^{3+} \quad (1)$$

or if more correctly written according to a Kroeger−Vink notation

$$2Mn^{x}_{Mn} + 2RuO_2 \leftrightarrow 2Ru^{\bullet}_{Mn} + 2e^{-} + Mn_2O_3 + 0.5O_2 \quad (2a)$$

$$Mn^{x}_{Mn} + e^{-} \leftrightarrow Mn^{-}_{Mn} \quad (2b)$$

$$Mn^{\bullet}_{Mn} + e^{-} \leftrightarrow Mn^{x}_{Mn} \quad (2c)$$

Note that these equations do not imply the formation of any point defect (except for the substitutional defect), but only the occurrence of a redox reaction between Mn and Ru ions. In particular, eq 2b indicates the possible reduction of Mn^{3+} to Mn^{2+}, while eq 2c is relative to the reduction of Mn^{4+} ions to Mn^{3+}.

The model suggested by Raveau is able to explain the FM interaction between the *newly* generated Mn^{3+} and the Mn^{4+} when the starting material is AF and constituted by only tetravalent ions such as $CaMnO_3$. In addition, the same authors

* To whom correspondence should be addressed. E-mail: lorenzo.malavasi@unipv.it.

† Dipartimento di Chimica Fisica "M. Rolla", INSTM, IENI/CNR Unità di Pavia, Università di Pavia.

‡ CNISM and Dipartimento di Fisica "A. Volta", Università di Pavia.

10.1021/jp052423z CCC: $30.25
Published on Web 10/14/2005

indicate the possible valence fluctuation

$$Mn^{4+} + Ru^{4+} \rightarrow Ru^{5+} + Mn^{3+} \quad (3)$$

as a source of FM interaction between Ru and Mn ions and by considering a possible hybridization between the Ru^{5+} and Ru^{4+} (electronic configurations t_{2g}^3 and t_{2g}^4, respectively) empty e_g orbitals and the Mn^{3+} orbitals, thus directly participating in a FM exchange.

Other authors[8,10,11] suggest that the metal−insulator (M−I) transitions and the magnetoresistance (MR) behavior found in Ca-doped $LaMnO_3$ can be understood in the framework of phase separation and coexistence of two FM and M phases: one Ru^{4+} rich with FM coupling between Ru and Mn ions and another (with the FM transition at a lower temperature and poor conducting in the magnetic phase) characterized by the presence of Ru^{3+} ions AF-coupled with neighboring Mn ions. This overall picture indicates that, up to now, a clear explanation of the *real* effect caused by Ru ion when entering the perovskite structure is still lacking.

We previously carried out thorough studies on Na-doped manganites as a function of composition (x), oxygen content (δ), and preparation route.[12−17] Therefore, to understand and deepen the role of Ru substituted at the Mn site, we started a thorough study on the $La_{1-x}Na_xMn_{1-y}Ru_yO_{3+\delta}$ system (LNMRO) with optimal cation doping, i.e., with an average Mn valence state of ∼3.30, and with weaker cation doping.

We also stress that our previous X-ray absorption spectroscopy (XAS) investigation of this system[18] demonstrated that the ruthenium is present, in hole doped mixed-valence manganites of the $La_{1-x}Na_xMnO_{3+\delta}$ system, with a mean valence state of no more than +4. XAS measurements clearly indicated that a simple Mn reduction (eqs 2a−c) is not the only mechanism involved in charge compensation when Ru is introduced into the manganite lattice, also according to the absence of a Mn valence state lower than +3. We then suggested that cation vacancy compensation through

$$2Mn_{Mn}^{x} + 2RuO_2 \leftrightarrow 2Ru_{Mn}^{\bullet} + O_O^x + \frac{1}{3}V_{Mn}'''' + \frac{1}{3}V_{La}''' + Mn_2O_3 \quad (4)$$

acts, in particular at a relatively low intrinsic hole doping ($x = 0.05$), to keep the system neutral, while at higher hole concentrations, a more direct electron exchange between Mn^{3+}/Mn^{4+} and Ru^{3+}/Ru^{4+} couples is present. In both cases, the mechanisms involved ensure the prevention of an overly strong manganese reduction. Moreover, an efficient redox system is present in the $x = 0.15$ samples which allows us to keep the average Mn valence state nearly constant, even though it is lower than that of the Ru-free compound.

In a previous communication,[19] we showed how the currently suggested charge compensation mechanisms for Ru doping fail to account for all the properties of these samples. In this extended work, we report a more complete structural, electrical, and magnetic characterization on the LNMRO system, also comprising an investigation of the role of the oxygen content in the related redox properties. The experimental investigation has been realized with the aid of several techniques such as X-ray powder diffraction (XRPD), electron microprobe analysis (EMPA), thermogravimetry (TG), electrical resistivity and magnetization measurements, and electron paramagnetic resonance (EPR).

2. Experimental Section

Samples of the $La_{1-x}Na_xMn_{1-y}Ru_yO_{3+\delta}$ (LNMRO) system were prepared with $x = 0.05$ and 0.15 and $y = 0$, 0.05, and 0.15 by a solid-state reaction starting from La_2O_3 (Aldrich, 99.999%), Mn_2O_3 (Aldrich, 99.999%), Na_2CO_3 (Aldrich, 99.99%), and Ru_2O_5 (Aldrich, 99.99%). Pellets were prepared from the thoroughly mixed powders and allowed to react at 1233 K for at least 90 h, during which they were reground and repelletized at least twice. Low reaction temperatures and long firing times have been chosen to ensure that no Na evaporates during the synthesis.[12]

After synthesis, two batches of the as-prepared samples were annealed for 72 h at 1173 K in oxygen and in argon, and the reactions were quenched at room temperature in an ice/water mixture.

XRPD patterns were acquired on a Bruker "D8 Advance" diffractometer equipped with a Cu anticathode, a graphite monochromator on the diffracted beam, and a proportional detector. Measurements were carried out in the angular range from 10° to 120° with a step size of 0.02° and a counting time of 10 s per step. Diffraction patterns were refined by means of the Rietveld method with the FullProf software.[20]

EMPA measurements were carried out using an ARL SEMQ scanning electron microscope, performing at least 10 measurements in different regions of each sample. According to EMPA and XRPD data, the synthetic procedure described above gave single-phase materials; in addition, each sample was found to be highly homogeneous in the chemical composition, which was in good agreement with the nominal one.

In TG measurements, performed to determine the weight variation of the samples when exposed to different atmospheres, the samples underwent the following treatments: (i) a 10 K/min ramp in oxygen, (ii) an isothermal step at 1073 K in oxygen for 360 min, (iii) a 10 K/min ramp in oxygen down to 423 K, and (iv) a 10 K/min ramp in argon up to 1173 K.

During steps (i) and (ii), the samples were allowed to equilibrate with the oxygen atmosphere and increase their oxygen content by an amount δ; in addition, with the reduction in temperature during step (iii), the maximum δ value, relative to these experimental conditions, is achieved. Finally, step (iv) in argon induces the system to equilibrate under the new conditions, thus leading to a loss of oxygen.

Absolute values of oxygen contents were determined by means of chemical analysis on some selected samples through the commonly used titration with potassium permanganate[21] and through previous thermogravimetric results on the Ru-undoped samples. We remark, however, that the presence of two redox couples makes the definition of the oxygen content a quite hard task. So we are aware of an average relative error of 5−10% on the δ values presented. Let us note that the observed weight variations are related to the bulk and not to the surface, because of the extremely low value of the surface area.

Static magnetization was assessed at different applied fields in the temperature range of 2−350 K with a SQUID magnetometer (Quantum Design). Field dependence of magnetization was also investigated at 2 K for a field ranging between 0 and 7 T.

Resistivity and MR measurements were carried out between 320 and 10 K at 0, 1, and 7 T magnetic fields with the DC-four electrodes method by means of a specific probe directly inside the magnetometer. Complementary EPR measurements were performed in X-band (∼9.5 GHz) to study the temperature dependence in the range of 300−470 K.

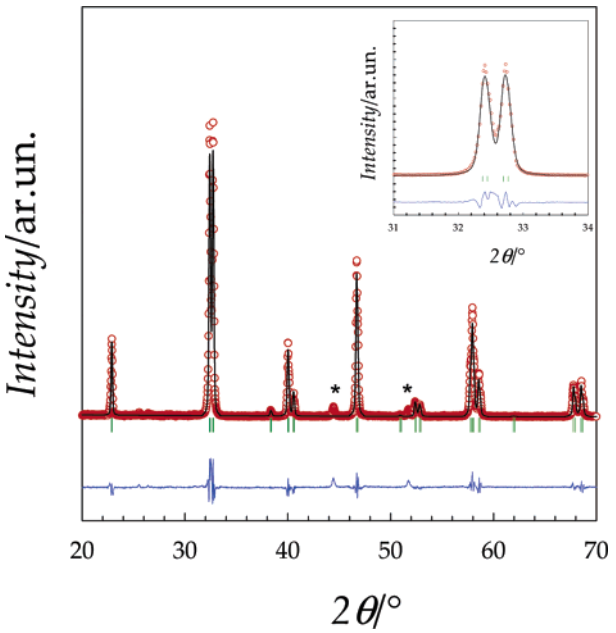

Figure 1. Rietveld refined X-ray pattern of the $La_{0.95}Na_{0.05}Mn_{0.95}Ru_{0.05}O_{3+\delta}$ (N5R5O) sample annealed in pure oxygen. In the inset, the region around the most intense peak is magnified. The asterisks correspond to the reflections coming from the sample holder.

3. Results

1. X-ray Powder Diffraction (XRPD). XRPD patterns were collected on all the LNMRO samples for both oxygen and argon thermal treatments. As a selected example, Figure 1 reports the Rietveld refined pattern of the $La_{0.95}Na_{0.05}Mn_{0.95}Ru_{0.05}O_{3+\delta}$ sample annealed in oxygen, hereafter named N5R5O. The crystal structure is rhombohedral and belongs to the *R*-3*c* space group (no. 67). The lattice constants, cell volumes, crystal structure, and oxygen content for this sample and for all the others are listed in Table 1.

All the samples treated in oxygen, irrespective of the Na or Ru doping, possess a rhombohedral structure. Looking at the $x = 0.05$ series, we notice that the $a(c)$ parameter has a minimum (maximum) that corresponds to the Ru = 0.05 sample. On the other hand, for the $x = 0.15$ series, an overall expansion of both parameters occurs by increasing the level of Ru doping.

The treatment in argon causes, for the $x = 0.05$ series, the material to adopt an orthorhombic structure (e.g., *Pbnm*), while for the $x = 0.15$ series, only the $y = 0.15$ sample becomes orthorhombic and the others remain rhombohedral. With regard to the $x = 0.05$ series, it can be noticed that the orthorhombic distortion is more severe (O′) for the undoped and $y = 0.15$ samples ($b/a < \sqrt{2}$), while the common O distortion ($b/a > \sqrt{2}$) pertains to the $y = 0.05$ compound. Let us recall that in the O′ phase a cooperative and static Jahn−Teller distortion, resulting from the e_g ($x^2 - y^2$) orbital ordering, leads to the expansion of the unit cell in the basal plane.

In Table 1, the volume (V) for all the samples is reported. For both series, the argon treatment causes a general increase in V as a consequence of the reduction of both Mn and Ru ions.[18] In more detail, for the $x = 0.05$ samples annealed in pure oxygen, only a slight variation of V is found as the Ru content (y) increases while a first decrease followed by an increase is observed for the $x = 0.05$ samples annealed in argon. A more "easy" V trend is found for the $x = 0.15$ samples since for both the annealing treatments V increases by increasing y.

2. Resistivity and Magnetoresistivity. With respect to the $x = 0.05$ samples annealed in oxygen, the Ru-free sample (N5O) is semiconducting (S) while the addition of Ru effectively reduces the resistivity of the samples (also inducing the S−M transition), as previously shown.[19] After applying a magnetic field, we found no significant variation in ρ for the N5O sample while an appreciable effect was observed for the N5R5O and N5R15O samples. The $\rho(T)$ curves at 0, 1, and 7 T and the correspondent MR(T) curves for these two samples are plotted in panels a and b of Figure 2, respectively. The MR values were calculated according to

$$\mathrm{MR}(\%) = \frac{R(H) - R(0)}{R(0)} \times 100 \qquad (5)$$

For the N5R5O sample, the magnetic field strongly reduces the resistivity, with an evident MR effect at a T value corresponding to the S−M transition at higher temperatures, while no clear MR behavior is detectable in connection with the wide bump in the $\rho(T)$ curve. For N5R15O, the application of a magnetic field allows detection of the two transitions seen as a shoulder in the $\rho(T)$ curves. All the argon-annealed samples with $x = 0.05$ are insulators with very high ρ values and with negligible MR effects. We just stress that also in this case the Ru-doped samples have ρ values that are lower than the Ru-free ones.

Let us now consider the $x = 0.15$ samples. For all the oxygen-annealed ones, an S−M transition is present, as shown in Figures 3a,b and 4a. From these curves, we can deduce, as a common trend, an increase in $\rho(T)$ and a decrease in the transition temperature T_{SM} with an increase in y. The argon-annealed samples of the $x = 0.15$ series generally exhibit a T_{SM} decrease or a semiconducting behavior. Nevertheless, an interesting MR effect is observed for N15R15Ar, which also shows an increase in T_C (see later) with reducing condition annealing. For N15R15Ar, the MR, plotted in Figure 4b together with the

TABLE 1: Sample Formulas, Annealing Treatments, Crystal Structures (R, rhombohedral; O, orthorhombic), Lattice Parameters (*a*, *b*, and *c*), Cell Volumes (*V*), Oxygen Contents (*δ*), and Curie Temperatures (T_c), for the Samples Considered in the Paper

sample	treatment	structure	*a* (Å)	*b* (Å)	*c* (Å)	*V* (Å^3)	*δ*	T_C (K)
$La_{0.95}Na_{0.05}MnO_3$	oxygen	R	5.5241(2)	5.5241(2)	13.3417(2)	58.75(1)	0.078	117
$La_{0.95}Na_{0.05}Mn_{0.95}Ru_{0.05}O_3$	oxygen	R	5.5212(2)	5.5212(2)	13.3501(3)	58.744(1)	0.04	251
$La_{0.95}Na_{0.05}Mn_{0.85}Ru_{0.15}O_3$	oxygen	R	5.5263(2)	5.5263(2)	13.3455(2)	58.824(2)	0.058	212
$La_{0.95}Na_{0.05}MnO_3$	argon	O	5.5445(1)	7.7574(2)	5.5864(2)	60.051(1)	0.01	112
$La_{0.95}Na_{0.05}Mn_{0.95}Ru_{0.05}O_3$	argon	O	5.5153(2)	7.8082(2)	5.5154(2)	59.384(1)	0.072	182
$La_{0.95}Na_{0.05}Mn_{0.85}Ru_{0.15}O_3$	argon	O	5.5572(1)	7.7786(3)	5.5236(2)	59.753(2)	0.035	167
$La_{0.85}Na_{0.15}MnO_3$	oxygen	R	5.5044(1)	5.5044(1)	13.3317(2)	58.292(2)	0	305
$La_{0.85}Na_{0.15}Mn_{0.95}Ru_{0.05}O_3$	oxygen	R	5.5123(2)	5.5123(2)	13.3392(2)	58.487(1)	−0.02	301
$La_{0.85}Na_{0.15}Mn_{0.85}Ru_{0.15}O_3$	oxygen	R	5.5187(1)	5.5187(1)	13.3454(2)	58.645(2)	0.01	172
$La_{0.85}Na_{0.15}MnO_3$	argon	R	5.5094(3)	5.5094(3)	13.3363(2)	58.417(1)	−0.01	265
$La_{0.85}Na_{0.15}Mn_{0.95}Ru_{0.05}O_3$	argon	R	5.5179(2)	5.5179(2)	13.3461(2)	58.644(2)	0.05	266
$La_{0.85}Na_{0.15}Mn_{0.85}Ru_{0.15}O_3$	argon	O	5.5246(2)	7.8091(3)	5.52191(2)	59.547(2)	0.035	189

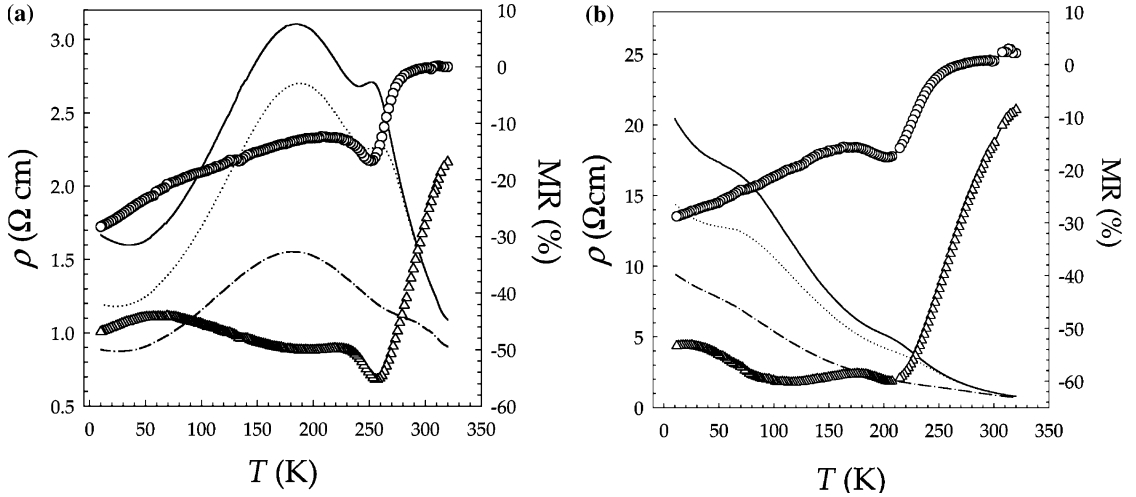

Figure 2. Resistivity curves for the N5R5O (a) and N5R15O (b) samples measured at null applied magnetic field (0 T, —) and at 1 (···) and 7 T (—·—). MR curves at 1 (○) and 7 T (△) are also plotted (see the scale on the right *y*-axis).

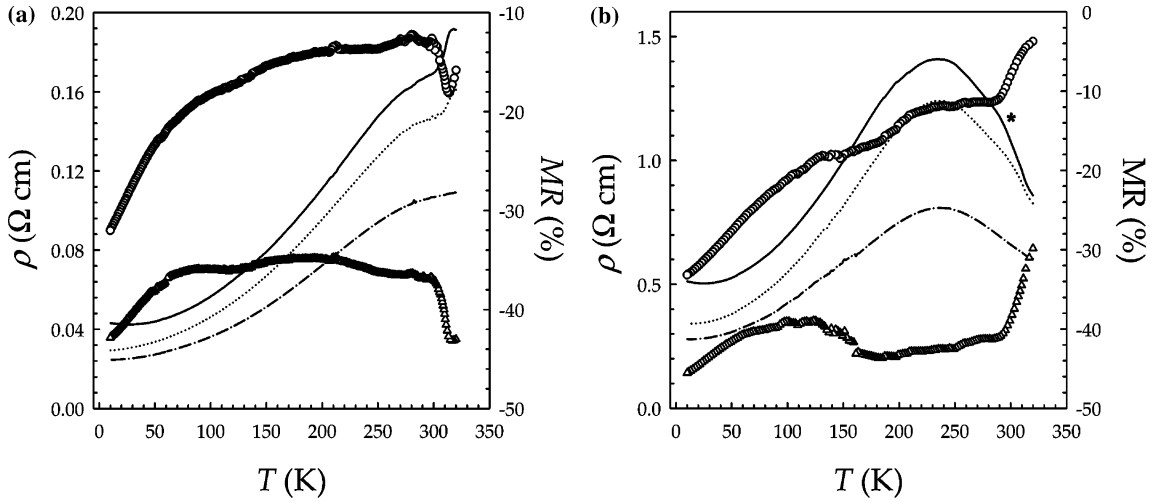

Figure 3. Resistivity curves for the N15O (a) and N15R5O (b) samples measured at null applied magnetic field (0 T, —) and at 1 (···) and 7 T (—·—). MR curves at 1 (○) and 7 T (△) are also plotted (see the scale on the right *y*-axis).

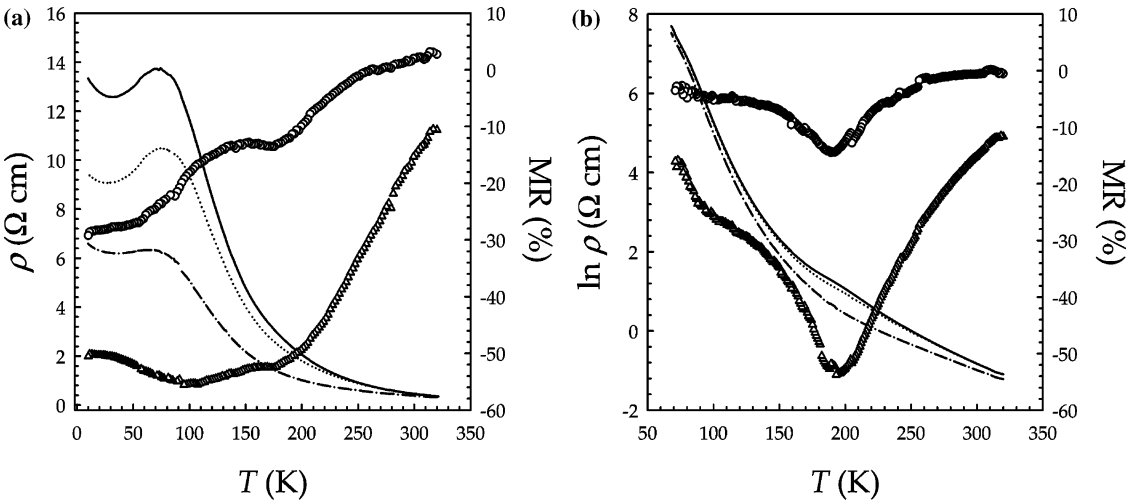

Figure 4. Resistivity curves for the N15R15O (a) and N15R15Ar (b) samples measured at null applied magnetic field (0 T, —) and at 1 (···) and 7 T (—·—). MR curves at 1 (○) and 7 T (△) are also plotted (see the scale on the right *y*-axis).

related ln $\rho(T)$ curves at 0, 1, and 7 T, shows a clear peak around 200 K, whose position slightly moves toward a higher T with an increase in the magnetic field. In a manner different from that of all the other samples, a net decrease in the MR response is observed before and after the peak.

3. Magnetic Measurements. Figure 5a reports the zero-field cooling (ZFC) and field cooling (FC) molar susceptibility χ_{mol} versus T curves at 100 Oe for the $x = 0.05$ samples annealed in oxygen. All the samples show clear transitions from a paramagnetic (P) to a ferromagnetic (F) state. The Curie

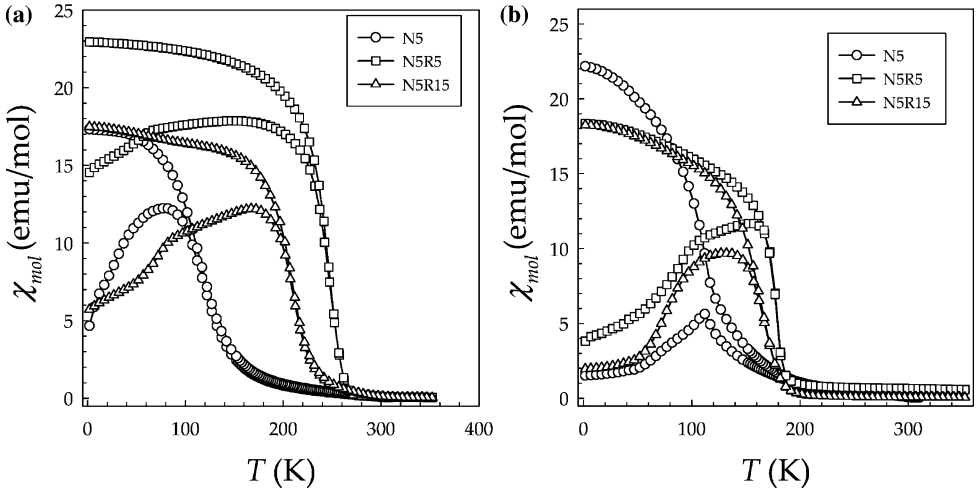

Figure 5. ZFC and FC curves for (a) oxygen- and (b) argon-annealed $La_{0.95}Na_{0.05}Mn_{1-y}Ru_yO_{3+\delta}$ samples with $y = 0$ (circles), 0.05 (squares), and 0.15 (triangles).

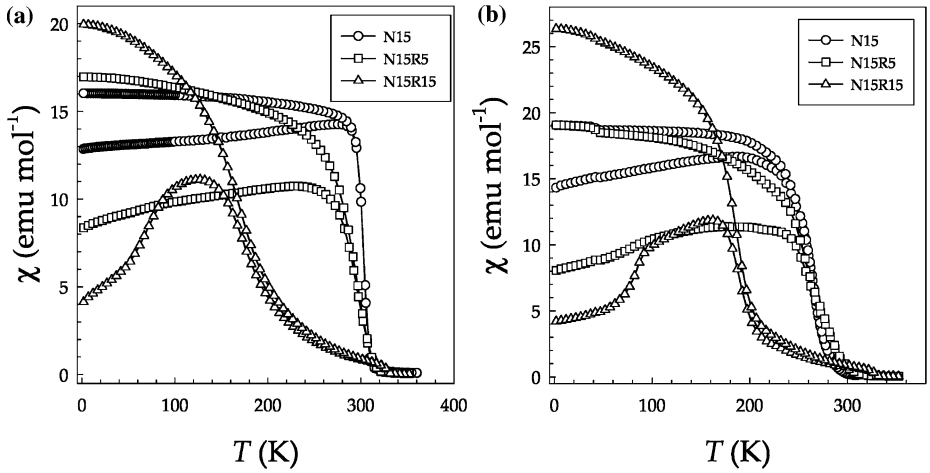

Figure 6. ZFC and FC curves for (a) oxygen- and (b) argon-annealed $La_{0.85}Na_{0.15}Mn_{1-y}Ru_yO_{3+\delta}$ samples with $y = 0$ (circles), 0.05 (squares), and 0.15 (triangles).

temperatures (T_C), taken at the inflection points on the FC curves, are reported in Table 1: the lowest T_C corresponds to the Ru-undoped sample. Significant deviation between the FC and ZFC curves occurs, thus indicating the presence of small magnetic domains possibly connected with magnetic nonhomogeneity[12] related to the large δ values and, consequently, to the presence of a large amount of cation vacancies. Indeed, the N5R5 sample shows the best characteristics, despite the lowest Mn average valence according to the XAS data.[18]

In Figure 5b, the analogous curves after argon annealing are reported. For the Ru-undoped sample, T_C is practically unchanged, while for the other two samples, T_C is reduced by ~70 K (N5R5) and ~45 K (N5R15), respectively. The decrease in T_C for this series with respect to the oxygen-annealed one has to be ascribed to a general decrease in the Mn average valence state, as indicated by XAS data. Besides, the orthorhombic structure and a generally higher cell volume, corresponding to the presence of a larger amount of Ru^{3+}, can hinder the magnetic interactions with respect the corresponding oxygen-annealed samples. For both oxygen- and argon-annealed samples, however, the sharpest PF transition with the highest T_C values occurs for N5R5.

The $x = 0.15$ series is characterized by higher T_C values and sharpest magnetic transitions with respect to the $x = 0.05$ series. In Figure 6a, the FC and ZFC curves at 100 Oe for the $x = 0.15$ samples annealed in oxygen are reported. A progressive T_C reduction with an increase in the level of Ru doping together with a widening of the PF transition and increased difference between the FC and ZFC curves can be noticed. For these samples, the presence of Ru^{4+} (according to XAS results) is indeed mainly related to a progressive increase in the oxygen overstoichiometry, thereby giving rise to progressive magnetic nonhomogeneity in the samples. The argon treatment causes a T_C reduction for the undoped sample and the N15R5 sample and, on the other hand, an increase for the N15R15 one (Figure 6b). The sharper PF transition and the higher T_C value of this sample with respect to those of the analogous oxygen-annealed one suggest again the important role of the cation vacancies in the magnetic properties of these compounds (δ is reduced by ~30% with respect to that of the N15R15O sample).

For all the considered samples, saturation of the magnetization was reached at 2 K by applying a magnetic field up to 7 T. The magnetic moment value per unit formula obtained from magnetization saturation is in good agreement (with an error of <10%) with the expected ones from the stoichiometric formula, considering $S = 0$ for Ru^{4+} ions. A further improvement in the agreement is obtained considering the vacancy formation mainly on the B site, as suggested by neutron diffraction results found in the Na-doped manganites.[22]

To investigate the magnetic (and chemical) homogeneity of the samples and to obtain information about the character of ruthenium/manganese substitution, EPR measurements were

performed. The Ru-undoped samples showed the typical lanthanum manganite spectrum, already observed and described in refs 12, 23, and 24. For all the investigated samples, a signal with a g factor of $\cong 2$ is present at room temperature, due to Mn^{4+} or $Mn^{3+}-Mn^{4+}$ Zener pairs. In many cases, a second component can be detected with an effective g factor, g_{eff}, higher than 2 that moves toward $\cong 2$ with an increase in temperature. This suggests the presence of sample regions with different long-range magnetic interactions, these regions merging more or less rapidly according to the sharpness of the PF transition. EPR signals related to ruthenium are not clearly observable in all the samples. For the N5 samples, a structured $g > 2$ signal is present, while for the N15 samples, this signal is present only after argon annealing. These data can agree with the XAS results[18] by considering that Ru^{4+} is not EPR active and ascribing the structured signal to Ru^{3+}.

Starting from the data previously obtained for the Ru-undoped compounds, we developed an evaluation of the Mn^{4+} content of these samples by comparing the EPR intensities (areas) at 470 K, i.e. in the paramagnetic phase, and taking into account the dependence of the EPR intensity on the T_C values. A very good agreement can be found with XAS results when considering the low Ru content ($\leq 5\%$), whereas some discrepancies are revealed for the samples with the highest Ru content where this procedure ended up with an estimation of the Mn^{4+} amount of $<30-35\%$ with respect to the one determined from XAS data. The reason for these differences can be related to the different temperatures considered for XAS (room temperature) and EPR (470 K) data, particularly if the internal redox reaction

$$Mn^{4+} + Ru^{3+} \rightarrow Mn^{3+} + Ru^{4+} \qquad (6)$$

may occur at 470 K, thus affecting the EPR intensity. However, this last point will be the object of future research aimed at defining any possible valence fluctuation at high T or other effects that may lead to this discrepancy for only the Ru = 0.15 samples.

4. Discussion and Conclusion

In this paper, we present the results of an investigation of the structural, electrical, and magnetic properties of the $La_{1-x}Na_xMn_{1-y}Ru_yO_{3+\delta}$ system (LNMRO) with optimal cation doping ($x = 0.15$) and with a lower level of cation doping ($x = 0.05$).

Several parameters affect the properties of this system that can be considered, then, a *complex* system. (i) Na doping, which broadens the conduction band by creating holes. (ii) Ru doping, which on one hand contributes positively to the DE−FM exchange thanks to the availability of e_g orbitals, in particular when it is diluted in the B sublattice, while for higher concentrations, we may expect SE (super exchange)−AF coupling between Mn^{3+} and Ru^{n+} ions. On the other hand, Ru doping involves the Mn reduction and/or the oxygen content increase which in turn means an increase in the cation vacancy concentration; moreover, a broadening of the conduction band may be expected due to the more expanded nature of the 4d orbitals of Ru. (iii) Oxygen content, which, as already recognized for Ru-free materials, is a key factor in manganites but here plays an additional role being involved in partial or total Ru compensation. In addition, holes and electrons created by oxygen over- or understoichiometry were shown to affect in a nontrivial way the redox couples present in the LNMRO series. (iv) e_g occupation, which may play a fundamental role in determining the possible hole hopping between Zener ions. All the Ru ions, irrespective of their oxidation state, have unoccupied e_g orbitals and can be regarded as Mn^{4+} ions. Nevertheless, possible AF interaction between Mn^{4+} and Ru^{n+} ions may become progressively significant for high levels of Ru doping and high Mn valence states.

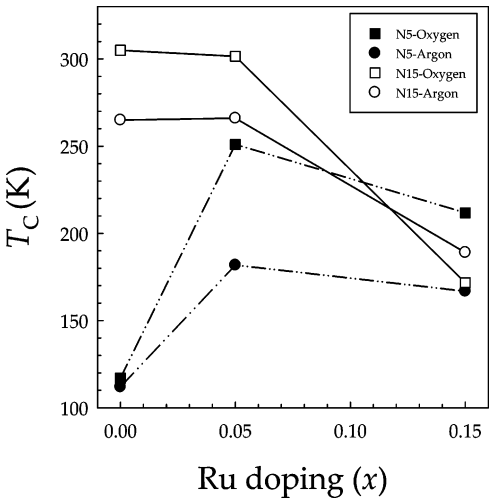

Figure 7. Curie temperatures (T_C) as a function of Ru doping for all the samples considered. See the legend for details.

However, this list is not exhaustive since, for example, the role of ion mismatch on both the A and B sites was not taken into account. We will try, in the following discussion, to highlight which are the most important effects for the different series of samples that were studied.

Let us start with Na = 0.05 samples annealed in pure oxygen. As shown in Figure 7, the maximum T_C (251 K) was found for an intermediate level of Ru doping (0.05), while the Ru-free sample has a T_C lower by more than 100 K and the Ru = 0.15 sample by ~40 K, notwithstanding the fact that these last two samples have a Mn average valence higher than that of the Ru = 0.05 compound. A major role is then played here by cation vacancies and Ru doping. N5R5O has fewer cation vacancies with respect to both N5O and N5R15O compounds since part of the charge compensation due to the Ru doping is accomplished by partial internal Mn reduction. Moreover, with respect to the N5O sample, it contains Ru ions which contribute effectively in the enhancement of T_C. Differently, the N5R15O sample has more Ru but also more cation vacancies: the T_C difference between N5R5O and N5R15O samples is more or less the one expected for a difference of ~0.5% in vacancy concentration.[25] In this case, the effect of the interruption of the interaction path caused by the vacancies is also reflected in the insurgence of a semiconducting-like state for the N5R15O samples with respect to the N5R5O.

Let us note the presence of a double ρ transition in both these samples. Authors previously correlated it with a magnetic phase separation. The application of a magnetic field shifts at higher values the position of the first transition, namely, the one at a higher T, as usually found for S−M transitions, while it does not move the position of the second one. This suggests that this second transition may not be joined to a magnetic transition. We propose that the origin of this second "bump" in the $\rho(T)$ plot is actually related to the point defects connected to the compensation mechanism induced by the Ru doping. The effect caused be cation vacancies on the shape of $\rho(T)$ curves was already pointed out for LCMO and LNMO Ru-undoped systems[12,26] where disorder-induced localization phenomena were the source of the resistivity increase and of the appearance of shoulders in the curves.

The Na = 0.15 series shows nicely the direct role of charge compensation through the mechanism of eq 4 and partial internal redox reaction between Mn and Ru ions. The progressive reduction of the Mn valence state and the increase in the oxygen content cause the trend in the Curie temperatures observed in Figure 7. Ru doping causes the appearance of a bump in the $\rho(T)$ curve of the N15R5O sample and of a semiconducting-like regime for the higher Ru content. It is clear that for optimal doping, where all the hole doping is created through the extrinsic cation doping (Na), addition of Ru deteriorates the system properties. This happens because more and more cation vacancies are introduced along with the Ru doping. However, the Ru itself also does not "help" the system, in this case, since the hole doping is already optimal, and clearly, achieving the same amount of Zener ions with Mn ions only or with two different kinds of ions is not the same, thus suggesting that some size effect caused by the strong mismatch between Ru and Mn ions plays a role.

As a final comment on the argon annealing treatments, these were mainly performed to study the interplay between the redox couples present and the oxygen content variation. Ru seems to play a sort of buffer role, thus preserving the system from an overly strong reduction of Mn ions. This is more evident for the Na = 0.15 samples where the average Mn valence state between oxidizing or reducing thermal treatments is practically unchanged, while the valence of Ru ions is strongly shifted toward lower values. This is also the reason for the "unexpected" increase in T_C for the N15R15 sample after the annealing in the argon environment, where, as usual for manganites, we would have expected a T_C reduction. In this case, an interesting MR effect is also observed.

In the literature, together with the anomalous presence of two transitions in the $\rho(T)$ curves, the magnetic moment value per unit formula was also found to be significantly smaller that the expected one in CO−AFM manganites.[4] As we showed in the Results in the magnetic data, we found a good agreement between the expected and calculated magnetic moments by taking into account the exact nature of the samples, i.e., the cation stoichiometry, oxygen content, and Ru valence state. Therefore, we may suggest that discrepancy between calculated and experimental data may come from an incomplete analysis of all the sample features which, we recognize, may be difficult for these complex systems.

To conclude, the effect of ruthenium doping on the structural, transport, and magnetic properties of the $La_{1-x}Na_xMn_{1-y}Ru_yO_{3+\delta}$ compounds is not only directly related to the Ru/Mn substitution and to the Ru oxidation state but also indirectly connected to the oxygen content in the sample. Our data show that ruthenium addition can "improve" electrical and magnetic properties of nonoptimally (low) cation-doped semiconducting manganites, causing an increase in the T_C value and the insurgence of the MR effect, as observed for the N5R5O sample (MR ≅ 60% at 7 T and at ∼260 K).

This study has shown that to characterize these complex systems and extract meaningful physical information the full "chemical state" of all the samples, defined by the interconnected parameters cation composition, oxygen content, ion valence state, and spin state, must be known. Our study may be a starting point to suggest a proper way of gaining a full understanding of the effect of transition metal ion doping on the B site of manganites.

Acknowledgment. Dr. Simona Bigi is gratefully acknowledged for having performed EMPA analysis. The Department of Earth Science of Modena University and CNR of Modena are acknowledged for allowing SEM use. E. Jarosewich has kindly supplied the lanthanum standard for EMPA measurements. This work was founded by the Italian Ministry of the University and Research through the PRIN 2004 project.

References and Notes

(1) Cabeza, O.; Long, M.; Sevevac, C.; Bari, M. A.; Murihead, C. M.; Francesconi, M. G.; Greaves, C. *J. Phys.: Condens. Matter* **1999**, *11*, 2569.

(2) Raveau, B.; Maignan, A.; Mahendiran, R.; Khomskii, D.; Martin, C.; Hébert, S.; Hervieu, M.; Frésard, R. *J. Phys. Chem. Solids* **2002**, *63*, 901.

(3) Hébert, S.; Martin, C.; Maignan, A.; Retoux, R.; Hervieu, M.; Nguyen, N.; Raveau, B. *Phys. Rev. B* **2002**, *65*, 104420.

(4) Raveau, B.; Maignan, A.; Martin, C.; Hervieu, M. *J. Supercond.* **2001**, *14*, 217.

(5) Singh, B.; Sahu, R. K.; Manoharan, S. S. *J. Magn. Magn. Mater.* **2004**, *270*, 358.

(6) Autret, C.; Martin, C.; Maignan, A.; Hervieu, M.; Raveau, B.; Andre, G.; Bouree, F.; Kurbakov, A.; Trounov, V. *J. Magn. Magn. Mater.* **2002**, *241*, 303.

(7) Sahu, R. K.; Manoharan, S. S. *J. Appl. Phys.* **2002**, *91*, 7517.

(8) Vertruyen, B.; Flahaut, D.; Hébert, S.; Maignan, A.; Martin, C.; Hervieu, M.; Raveau, B. *J. Magn. Magn. Mater.* **2004**, *280*, 75.

(9) Battle, P. D.; Jones, C. W. *J. Solid State Chem.* **1989**, *78*, 281.

(10) Seetha Lakshmi, L.; Sridharan, V.; Natarajan, D. V.; Chandra, S.; Sankara Sastry, V.; Radhakrishnan, T. S.; Pandian, P.; Justine Joseyphus, R.; Narayanasamy, A. *J. Magn. Magn. Mater.* **2003**, *257*, 195.

(11) Seetha Lakshmi, L.; Sridharan, V.; Natarajan, D. V.; Rawat, R.; Chandra, S.; Sankara Sastry, V.; Radhakrishnan, T. S. *J. Magn. Magn. Mater.* **2004**, *279*, 41.

(12) Malavasi, L.; Mozzati, M. C.; Ghigna, P.; Azzoni, C. B.; Flor, G. *J. Phys. Chem. B* **2003**, *107*, 2500.

(13) Malavasi, L.; Mozzati, M. C.; Polizzi, S.; Azzoni, C. B.; Flor, G. *Chem. Mater.* **2003**, *15*, 5036.

(14) Malavasi, L.; Mozzati, M. C.; Ghigna, P.; Chiodelli, G.; Azzoni, C. B.; Flor, G. *Recent Res. Dev. Phys.* **2003**, *4*, 545.

(15) Bondino, F.; Platè, M.; Zangrando, M.; Zacchigna, M.; Cocco, D.; Comin, A.; Alessandri, I.; Malavasi, L.; Parmigiani, F. *J. Phys. Chem. B.* **2004**, *108*, 4018.

(16) Malavasi, L.; Mozzati, M. C.; Alessandri, I.; Depero, L. E.; Azzoni, C. B.; Flor, G. *J. Phys. Chem. B* **2004**, *108*, 13643.

(17) Ghigna, P.; Carollo, A.; Flor, G.; Malavasi, L.; Subias Peruga, G. *J. Phys. Chem. B* **2005**, *109*, 4365.

(18) Malavasi, L.; Mozzati, M. C.; Di Tullio, E.; Tealdi, C.; Flor, G. *Phys. Rev. B* **2005**, *71*, 174435.

(19) Malavasi, L.; Mozzati, M. C.; Tealdi, C.; Pascarelli, M. R.; Azzoni, C. B.; Flor, G. *Chem. Commun.* **2004**, *12*, 1408.

(20) Rodriguez-Carvajal, J. *Physica B* **1993**, *192*, 55.

(21) Yang, J.; Song, W. H.; Ma, Y. Q.; Zhang, R. L.; Sun, Y. P. *J. Magn. Magn. Mater.* **2004**, *285*, 417.

(22) Malavasi, L.; Ritter, C.; Mozzati, M. C.; Tealdi, C.; Islam, M. S.; Azzoni, C. B.; Flor, G. *J. Solid State Chem.* **2005**, *178*, 2042.

(23) Oseroff, S. B.; Torikachvili, M.; Singley, J.; Ali, S.; Cheong, S.-W.; Schultz, S. *Phys. Rev. B* **1996**, *53*, 6521.

(24) Causa, M. T.; Tovar, M.; Caneiro, A.; Prado, F.; Ibañez, G.; Ramos, C. A.; Butera, A.; Alascio, B.; Obradors, X.; Piñol, S.; Rivadulla, F.; Vázquez-Vázquez, C.; López-Quintela, M. A.; Rivas, J.; Tokura, Y.; Oseroff, S. B. *Phys. Rev. B* **1998**, *58*, 3233.

(25) Vergara, J.; Ortega-Hertogs, R. J.; Madruga, V.; Sapiña, F.; El-Fadii, Z.; Martinez, E.; Beltrán, A.; Rao, K. V. *Phys. Rev. B* **1999**, *60*, 1127.

(26) Malavasi, L.; Mozzati, M. C.; Azzoni, C. B.; Chiodelli, G.; Flor, G. *Solid State Commun.* **2002**, *123*, 321.